Schweizerischer Erdbebendienst
Service Sismologique Suisse
Servizio Sismico Svizzero
Swiss Seismological Service

ETH
Eidgenössische Technische Hochschule Zürich
Swiss Federal Institute of Technology Zurich

SITE CHARACTERIZATION REPORT

SKIES: Kriens, Schule (LU)

Dario Chieppa, Anastasiia Shinkarenko, Donat Fäh

Last Modification: 24th August, 2023

Schweizerischer Erdbebendienst (SED)
Service Sismologique Suisse
Servizio Sismico Svizzero
Servizi da Terratrembels Svizzer
ETH Zürich

Sonneggstrasse 5
8092 Zürich
Schweiz
dario.chieppa@sed.ethz.ch

Contents

Summary

Kriens (LU) is a village located south-west of Luzern in central Switzerland, in Canton Luzern. The place was chosen as site for the installation of the last station of Swiss Strong Motion Network (SSMNet) renewal project. In order to better assess the local subsurface, a passive seismic array is performed in and around the recently installed strong motion station of SKIES.

The results of the horizontal-to-vertical spectral ratio (H/V) analysis show two peaks. The peak at low frequency (1.07-1.34 Hz) is interpreted as the H/V fundamental peak and has two steep flanks with amplitude up to 8 This peak is found over the entire study area. The other peak, at higher frequency (4.82-10.42 Hz), is broader, has amplitudes lower than 2 and can be found only at the center of the study area and at north-west. This peak is interpreted as the H/V first higher mode peak.

The inversion of the passive seismic array data is performed using *dinver* and *Neopsy* techniques and allows the estimation of velocity profiles down to 800 m. *dinver* velocity profiles show a first interface at 8 m with V_s of about 72 m/s, a second interface at about 259 m with maximum V_s of 1360 m/s (SKES5l, SKES7l and SKES9l models) and a third one at about 800 m (V_s = 3250-3380 m/s), corresponding to the transition to the half-space. The Maximum A Posteriori (MAP) and the Maximum Likelihood (ML) models computed from *Neopsy* inversion show a gradual increase of shear-wave velocity with depth. The half-space is located at 100 m by MAP model and at 256 m by ML model. Quarter wavelength velocity approach (QWL, Joyner et al., 1981) estimates a maximum resolution of 136 m for picked dispersion and ellipticity curves which corresponds to an investigation depth which is much shallower than results of *dinver* and *Neopsy* inversions.

The V_{S30} for the site, calculated for *dinver* models, is 147.1 m/s, corresponding to soil class D in EC8 and SIA261 classifications. The theoretical shear-wave transfer function from the retrieved *dinver* profiles and that from MAP and ML models are similar over the entire frequency range and predict an amplification function which consists in a wide peak, at low frequency, followed by a slightly inclined trend where the average amplification is at about 3. The amplification ranges from 1.9 at 9.3 Hz to 9.6 at 1.9 Hz. Due to the recent installation, an amplification function curve is not yet available for the seismic station SKIES and cannot be compared with the computed SH-wave transfer function.

1 Introduction

The station SKIES is part of the Swiss Strong Motion Network (SSMNet). The station was installed on 20 July 2023 in the framework of the second phase of the Swiss Strong Motion Network (SSMNet) renewal project (Fig. 1). In order to better characterize the underground, to estimate the fundamental frequency of the site and the shear wave velocity, a passive array measurement was carried out on 25 July 2023.
The site is of interest for its location in a populated area close to the city of Luzern, to improve the network coverage around Vierwalderstättersee, and for the primary school in Kriens. From a geological point of view, SKIES seismic station is installed on peat and peatbog of Holocene age. Moving towards south-west, peat sediments change first in undifferentiated alluvial sediments and then into river gravel deposits.

Figure 1: Map showing the location of the strong motion station (blue triangle) in Kriens. Source: Federal Office of Topography.

2 Geological setting

A geological map of the surroundings of Kriens is shown in Fig. 2. Red dots represent the locations of the passive array; the blue triangle is the location of the station SKIES. Thirteen sensors are located on peat and peatbog sediments of Holocene age, two sensors are on undifferentiated alluvial sediments (Holocene) at the border with peat sediments towards north and river sediments towards south. The last sensor (SKES15) is on river gravel sediments (late Pleistocene – Holocene).

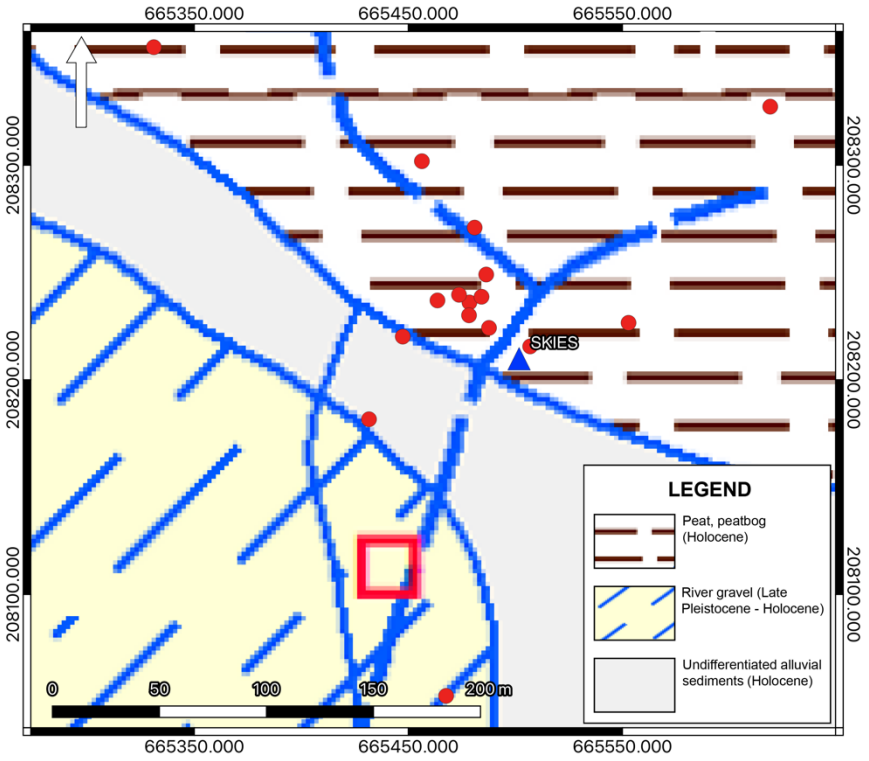

Figure 2: Geological map of the Kriens area. The stations of the passive array recordings are indicated by red dots, whereas the position of the strong-motion station SKIES is shown by a blue triangle. Source: Federal Office of Topography.

3 Passive site characterization measurements

3.1 Data set

To characterize the deep underground structure around the seismic station, a passive seismic measurement was performed in July 2023 by deploying an array of 16 stations (Fig. 4). The stations were planned to be located on five rings of different radii around a central station. The three stations of each ring were planned to be rotated 120 degrees one from the other and have radii of 6, 15, 35, 75 and 180 meters. Each ring, starting from the second, is rotated with respect to the inner ring of 30, 30, 20 and 40 degrees. The array central station (SKES01) is located around 35 m north-west from the permanent seismic station SKIES.

Each installation consisted of a Lennartz 5s sensor connected to a Centaur digitizer, with the exception of four stations in the central part which had two sensors connected to the same digitizer. The station names are composed of "SKES" followed by a two-digit number between 01 and 16. SKES02, SKES03, SKES04 and SKES06, in the inner rings, are connected to the second channel of Centaur digitizers; the remaining sensors are connected to the first channel. The array recording time was 210 minutes (12600 s). The station locations were measured by a differential GPS system (Leica Viva GS10) which was set up to measure with a precision better than 5 cm. The precision of measured points is below 5 cm.

Figure 3: Seismic station installation example for the measurements in Kriens.

Figure 4: Layout of the array measurement in Kriens. The locations of the stations for the passive seismic measurement are indicated by the red dots. The blue triangle indicates the seismic station site. Source: Federal Office of Topography.

3.2 H/V and RayDec ellipticity curves

Figure 5 shows H/V curves (left plot) determined using Geopsy software (Wathelet et al. 2020) and ellipticity curves (right plot) computed using the RayDec technique (Hobiger et al., 2009) for all measured sites.

Most of H/V curves show two peaks. The peak at low frequency, interpreted as the fundamental mode f_0, is marked by red crosses. The other is located at higher frequencies and is interpreted as the first higher mode peak (f_1 – blue crosses). f_0 is located in a restricted frequency range (1.07-1.34 Hz), is rather sharp and has two steep flanks. The peak amplitude ranges from 2.7 to 7.4. At certain stations the peak is well defined (e.g. SKES11); at other sites the f_0 peak appears as two close peaks (e.g. SKES01). f_1 is broad and symmetric, has gentle flanks and spans between 4.8 and 10.4 Hz with amplitude values between 0.96 and 1.88. SKES06 H/V curve shows a narrow and an unnatural trough to the left of the f_0 peak at about 0.68 Hz.

Maps in Fig. 6 show the areal distribution of f_0 (left) and f_1 (right) peaks. The frequency range for f_0 is rather narrow; lower frequencies can be observed at the center of the array for the three inner rings. Moving towards the outer rings, the frequency of the f_0 peak increases.

f_1 was picked at 10 sites in the center of the array and at SKES12 and SKES14 sites. As for the f_0 peak, the lowest frequencies are close to the center of the array.

The RayDec technique (Hobiger et al., 2009) is meant to eliminate the contributions of other wave types than Rayleigh waves and give a better estimate of the ellipticity. The RayDec ellipticity curves for all stations of the array show a pattern which is similar to the curves obtained with the

H/V analysis. Two well distinct peaks can be observed also for RayDec ellipticity curves. The dark green curve shows the RayDec ellipticity for the array central station (SKES01). The dark red curve represents the ellipticity for SKES09 seismic station, the closest station of the deployed array to the strong motion station SKIES. f_0 and f_1 peaks can be observed at both sites. Left flank of f_0 and its peak (1.07 Hz) coincide for SKES01 and SKES09 stations. The right flank presents some discrepancies in terms of shape up to 2 Hz. At higher frequencies, f_1 peak has different shapes: sharp with a trough below 1 for SKES09, broad with lower amplitudes for SKES01. The remaining RayDec curves are similar to SKES01 and SKES09 stations and to the H/V curves. Few curves present lower amplitudes both at low and high frequencies.

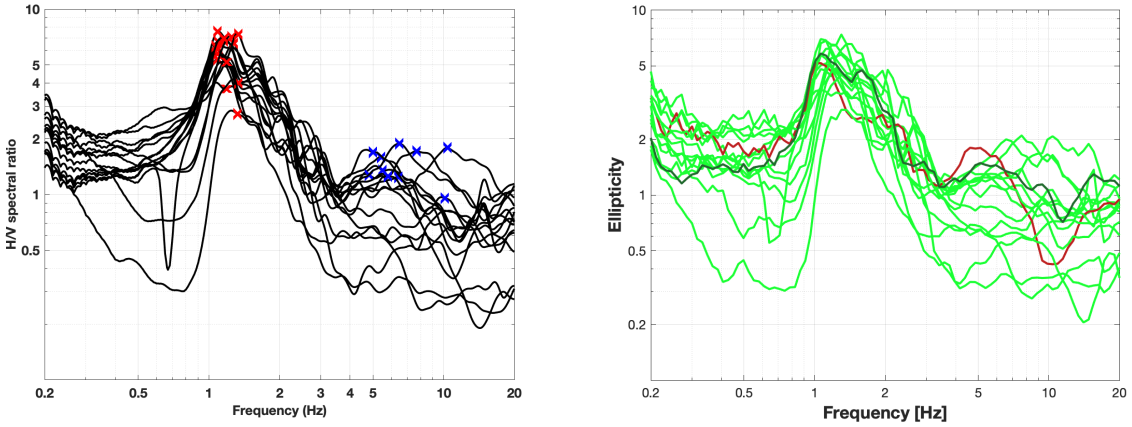

Figure 5: Left: H/V curves of the different stations of the array measurement in Kriens with picked fundamental frequency (red cross) and first higher mode (blue cross). Right: RayDec ellipticities for all stations of the array. The curve of SKES01, the array center, is highlighted in dark green, whereas the curve SKES09, linked to the measurement nearby the station is highlighted in dark red.

Figure 6: Map showing the variation in frequency for the H/V fundamental (left) and first higher (right) peaks over the area of Kriens, around the primary school. Source: Federal Office of Topography.

3.3 Polarization measurements

The polarization analysis was performed according to Burjánek et al. (2010) and Burjánek et al. (2012). The results for SKES01, the array center, and SKES09, the closest station to the SKIES station are shown in Fig. 7. From left to right we show: ellipticity, dip and strike. The two sites show the variability of the underground between the center of the array and one station in the third ring, towards south-west. The ground motion is linear polarized (~0.1) at 1 Hz at the center of the array, corresponding to the f_0 H/V peak. At lower and higher frequencies, the ground motion changes to quasi-elliptical (0.4) and remain such as till 30 Hz (Fig. 7 – left plot, top row). At SKES09, the ground motion is quasi-linear (0.2) at 0.2 Hz and almost linear at the H/V peak at about 1 Hz. Towards higher frequencies, the ground motion becomes elliptical (Fig. 7 – left plot, bottom row).

According to dip plots (central column – Fig. 7), seismic waves around SKES01 and SKES09 propagate parallel to the surface with a zero degree angle. The dip plot for the 14 remaining stations show horizontal ground motion over most of the frequency range. Only at two sites (SKES12 and SKES13), in the fourth ring, the ground motion is not horizontal between 0.2 and 0.5 Hz.

In the right column of Fig. 7 no predominant direction of polarization can be observed. For SKES01 station, two weak directions of polarizations can be observed: at about 1 Hz and at 4 Hz. Both directions are east-southeast west-northwest with a different angle (Fig. 7 – right plot top row). SKES09 station, instead, has a weak direction of polarization east-northeast west-southwest in the frequency range 0.2-0.6 Hz (right plot bottom row). The strike plot for the remaining stations doesn't show any predominant direction of polarization but weak directions changing from east-west (e.g. SKES14), to east-northeast west-southwest (e.g. SKES11) to west-northwest east-southeast (e.g. SKES10) at different frequencies.

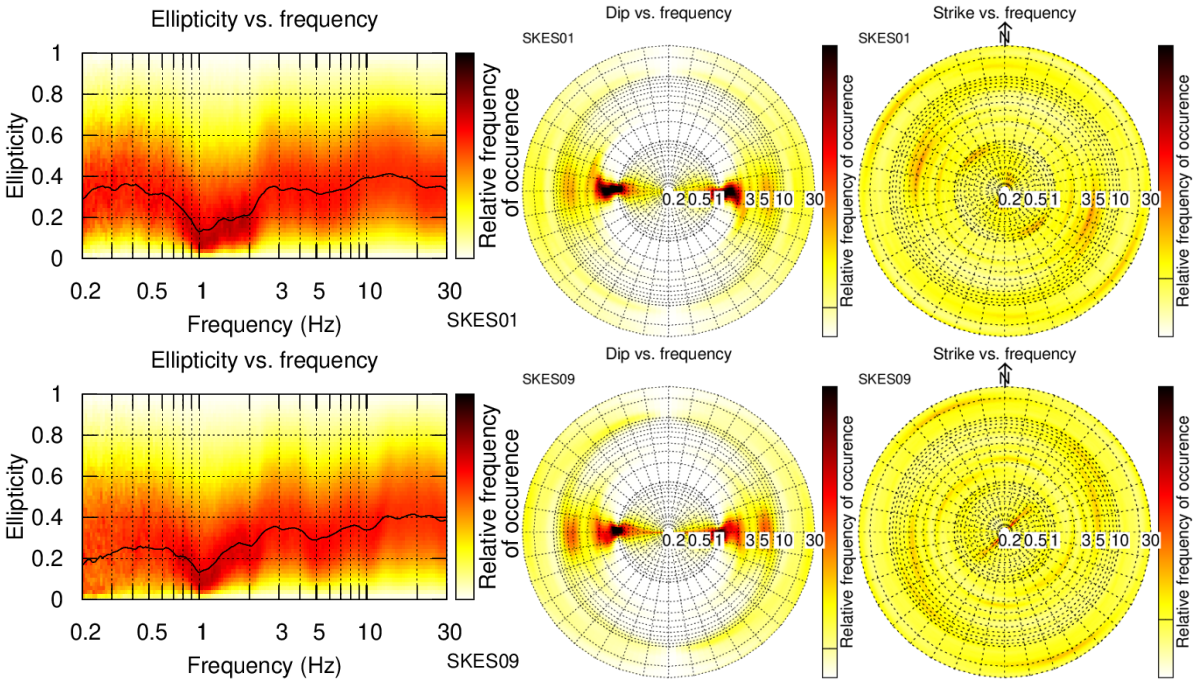

Figure 7: Polarization analysis of station SKES01 (top) and SKES09 (bottom).

3.4 3-component high-resolution FK

The results of the 3-component high-resolution FK analysis (Poggi and Fäh, 2010) are shown in Figs. 8 and 9. For Love waves, using the transverse component (top left plot – Fig. 8), one dispersion curve is picked between 1.2 and 9 Hz. The curve has three segments: steep (1.2-1.4 Hz), medium inclined (1.4-2.8 Hz) and flat (2.8-9 Hz). Surface-wave velocities decrease from 729 m/s at 1.2 Hz to 86 m/s at 9 Hz. Three dispersion curves are picked for the Rayleigh waves using vertical (2) and radial (1) components. For the vertical component the first curve is picked between 1.7 and 4.2 Hz and shows a straight and descending trend from 587 m/s to 170 m/s. The second curve is shorter and has a trend which is similar to the first curve. This curve is located at higher frequencies (3.9-6.3 Hz) and low wave velocity (117-68 m/s). The curve picked for the radial component stretches from 1.4 to 6.7 Hz. Its shape is more similar to that of transverse component than to the shape of dispersion curves for the vertical component and it is located at higher velocities. Over the same frequency range as the dispersion curves picked for the vertical and radial components, the ellipticity curves are picked (Fig. 9). The curves in the top row are picked for the vertical component. These two curves have different shapes: the left one, picked for the mode at low frequency, has a descending flank down to about 2.5 Hz changing into a flat portion with ellipticity values of 1; the right one is flat over the entire frequency range and has ellipticity close to 1. The curve on the bottom row of Fig. 9 is picked for the radial component. The picked ellipticity curve has a descending trend from 1.4 to 3.7 Hz, a trough and an ascending trend (up to 6.7 Hz).

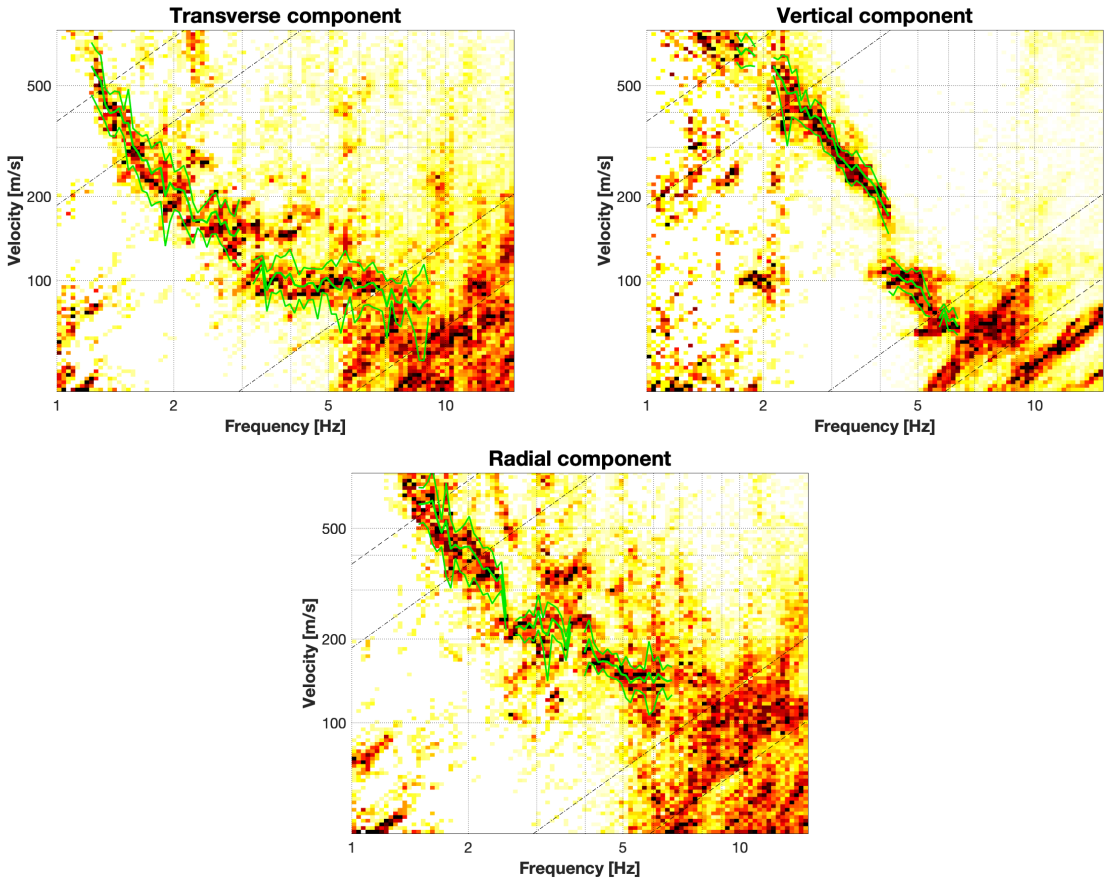

Figure 8: Dispersion curves for the transverse (top left), vertical (top right) and radial (bottom) components obtained with the 3-component HRFK algorithm (Poggi and Fäh, 2010). The dashed and dotted black lines are the array resolution limits. The solid and dashed green lines represent the data picking (central line) and the standard deviation (outer lines).

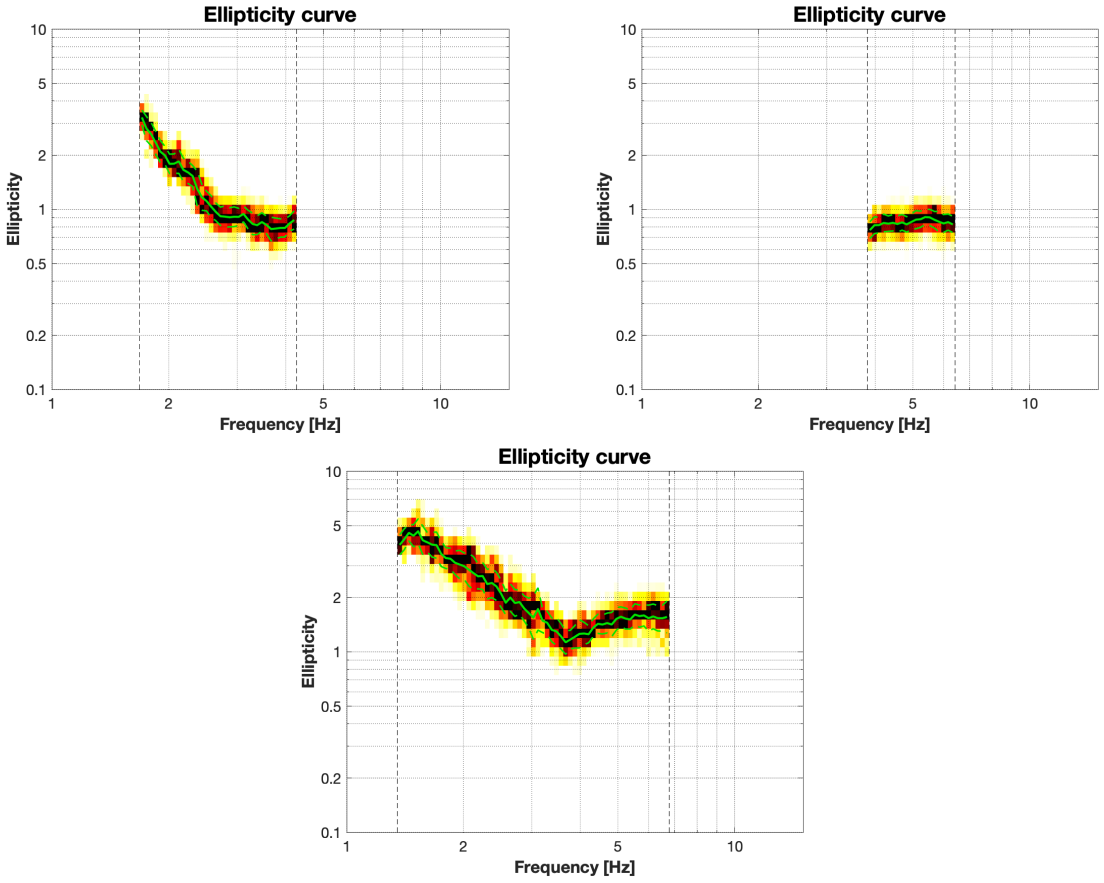

Figure 9: Ellipticity curves for the vertical (top row) and radial (bottom row) components using the 3-component HRFK algorithm (Poggi and Fäh, 2010). For the top row, left plot shows the mode picked at higher velocity; right plot is the mode at lower velocities. The dashed vertical lines represent the lower and upper frequencies for the picked dispersion curves. The solid and dashed green lines represent the data picking (central line) and the standard deviation (outer lines).

3.5 WaveDec

The results of WaveDec technique (Maranò et al., 2012) are shown in Fig. 10. This technique estimates the properties of single or multiple waves simultaneously with a maximum likelihood approach. In order to get good results, the parameter γ must be tuned to modify the sharpness of the wave property estimation between purely maximum likelihood estimation (γ=0) and a Bayesian Information Criterion (γ=1). Three tests are performed during this analysis changing the γ value. We tested γ equal to 0, 0.5 (corresponding to a mix of a maximum likelihood algorithm and a

Bayesian Information Criterion estimation) and 1. All three tests provide similar results. In the following we show the results using γ equal to 0.5, modelled Rayleigh waves, Love waves and seismic noise and a maximum of modelled waves equal to 3.
The picking of dispersion curves in WaveDec is performed in the wavenumber-frequency domain but it is here shown in the velocity-frequency domain for comparison with the results from other techniques (Fig. 10). Love-wave dispersion curve is continuously picked between 1 and 5.4 Hz (top left plot). It presents a steep sector and a flat portion. The first one extends down to 2 Hz and wave velocity velocities of 123 m/s; the other stretches between 2 and 5.4 Hz and *Vs* of about 90 m/s. The Rayleigh-wave dispersion curve is picked between 1.1 and 5.3 Hz (top right plot). The picked curve is rather straight over the entire frequency range. Wave velocity decreases from 764 to 69 m/s. The ellipticity angle curve for the picked Rayleigh-wave dispersion curve (bottom row) has positive values between 1.1 and 3.9 Hz changing into negative values up to 5.3 Hz. The shape of the ellipticity-angle curve shows a rather flat portion up to about 3 Hz followed by a steep descending flank. The particle motion for the picked dispersion curve is prograde below 3.9 Hz and retrograde above.

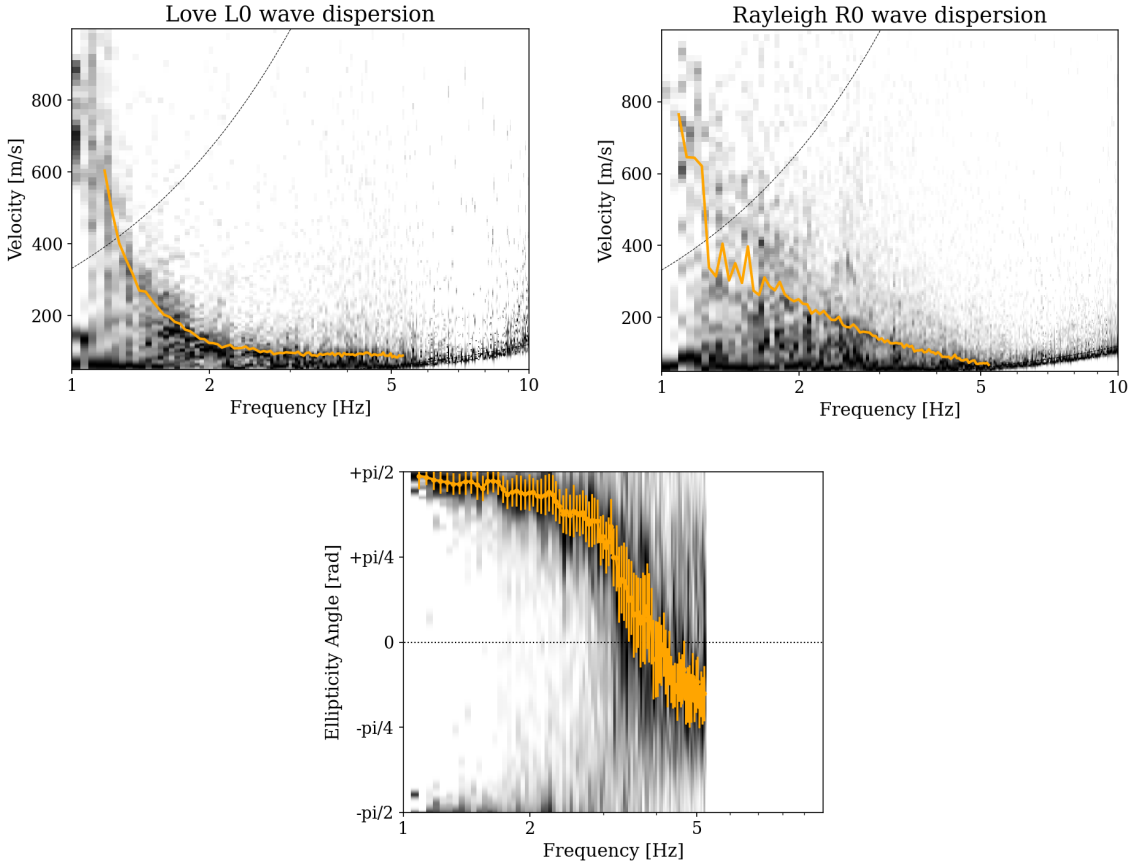

Figure 10: Dispersion curves for Love and Rayleigh waves (top row) and ellipticity angle curve for Rayleigh waves (bottom row) as obtained with WaveDec (Maranò et al., 2012). The dashed black lines (top rows) represent the array resolution limits, the solid orange line indicates the picked curve and the vertical bars at each frequency show the standard deviation for the ellipticity angle curves.

3.6 Modified SPatial AutoCorrelation

The SPAC (Aki, 1957) curves of the vertical components have been calculated using the MSPAC technique (Bettig et al., 2001) implemented in Geopsy (Wathelet et al., 2020). Rings with different radius ranges are defined and for all stations pairs with distances inside this radius range, the cross-correlation is calculated in different frequency ranges. These cross-correlation curves are averaged for all station pairs of the respective ring to give the SPAC curves. Rings are defined in such a way that at least three station pairs are located at about 120 degrees one from the other and their connecting vectors have a good directional coverage.

The results of MSPAC technique are shown in Fig. 11. The corresponding SPAC autocorrelation functions are shown in Fig. 12 for all selected rings. Black points indicate the data values which contributed to the final dispersion curve estimation, which was picked using the *spac2disp* function of the Geopsy. Two dispersion curves were picked for the Rayleigh waves (gray curves). The first mode, at lower velocity, is picked between 1.2 and 4.5 Hz. The second mode stretches between 1.9 and 4.6 Hz. These two curves are rather parallel and inclined towards higher frequencies.

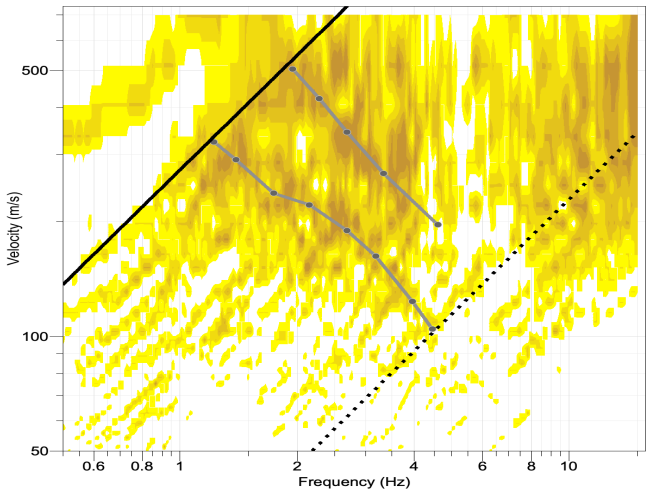

Figure 11: Rayleigh-wave dispersion curve obtained using spac2disp module of geopsy.

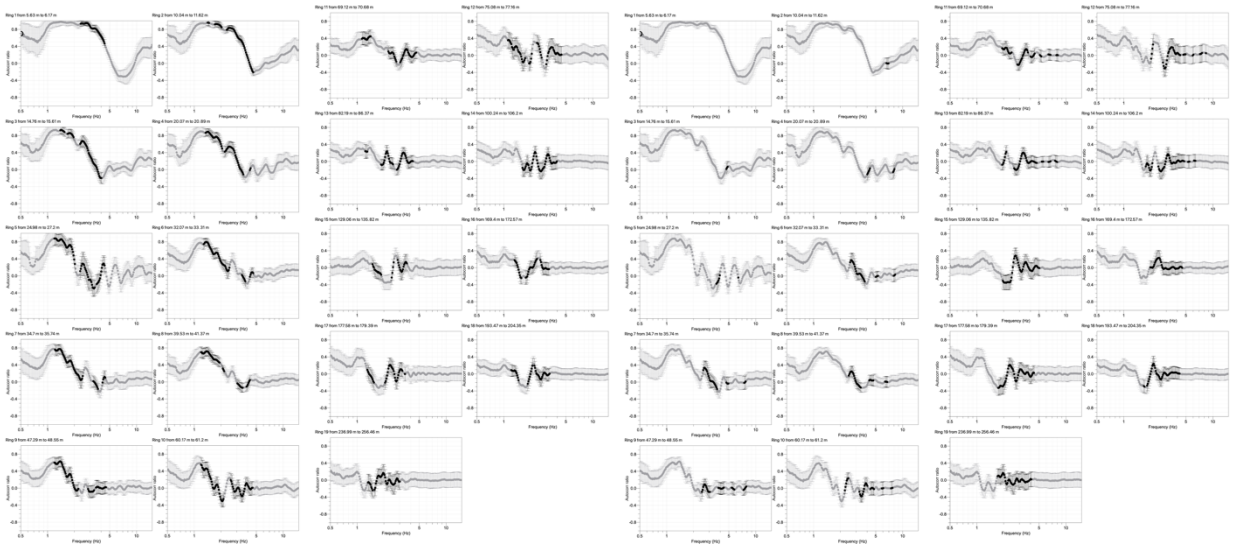

Figure 12: Autocorrelation functions for the mode at lower (left plot) and higher (right plot) velocities. The solid gray line represents the picked data; the black dashed and dotted lines indicate the array resolution limits.

3.7 Summary

Figure 13 gives an overview of Love- and Rayleigh-wave dispersion curves (left and central plots, respectively) and of the Rayleigh-wave ellipticity curves (right plot) determined using different processing techniques. For Love waves, WaveDec and 3C-HRFK techniques produce one dispersion curve each. The dispersion curve picked using 3C-HRFK shows a discontinuous curve stretching between 1.2 and 9 Hz. The curve picked by WaveDec technique is continuous, smoother, and with lower shear-wave velocities if compared to 3C-HRFK results. The two curves picked for Love waves (Fig. 13 – left plot) overlap only at low frequency, at about 1.2 Hz, and at high frequency, above 3 Hz.

The dispersion curves picked for Rayleigh waves are six: three for 3C-HRFK, one using WaveDec and two for MSPAC. The three curves picked using 3C-HRFK are computed using vertical (2) and radial (1) components and are shown in black and dark red colors, respectively. The picked curves do not overlap but show similarities in terms of shape and wave velocities. Rayleigh-wave dispersion curve for WaveDec technique (light blue) is close to the MSPAC dispersion curve at low velocity (gray) and to the second mode for 3C-HRFK (black). The three remaining curves, at higher velocities, are computed for radial and vertical components of 3C-HRFK, and the second mode of MSPAC. Among these three curves, the curve picked for the radial component is the one with lower velocity. Right plot of Fig. 13 shows the ellipticity curves of Rayleigh waves computed using RayDec, WaveDec and 3C-HRFK techniques. RayDec results are shown for SKES01 (dark green) and SKES09 (light green) stations, located in the center of the array and close to the permanent seismic station of SKIES. RayDec curves overlap between 0.7-1.1 Hz and show similar shapes at low and high frequencies. Ellipticity curve for radial component of 3C-HRFK technique overlap with RayDec curves along the right flank. Results for vertical component of 3C-HRFK perfectly connect and are continuous between 1.7 and 6.3 Hz. The shape of these ellipticity curves is similar to the right flank in RayDec curves but it is shifted at lower ellipticity values.

The ellipticity curve in light blue is picked using the WaveDec technique. This curve is converted from the picked ellipticity angle curve and consists in a descending flank between 1 and 4.1 Hz, probably the right flank of the main peak, a narrow trough and an ascending flank up to 5.3 Hz. The WaveDec curve doesn't overlap to the other curves but show similar shapes.

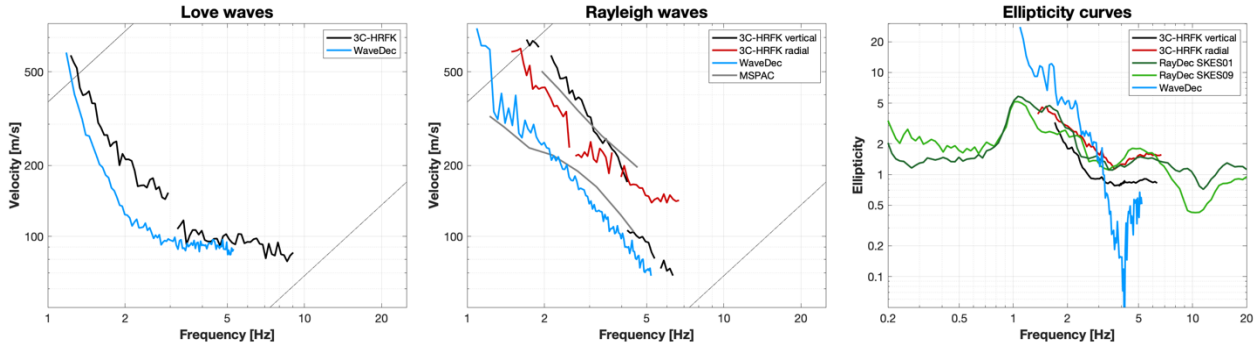

Figure 13: Comparison between the computed Love (left) and Rayleigh (center) wave dispersion curves and ellipticity curves (right).

4 Data inversion

4.1 Inversion targets

We performed an inversion combining the information of Rayleigh- and Love-waves dispersion curves and Rayleigh-wave ellipticity curve. The inversion involves one dispersion curve for Love waves (left plot – Fig. 14), two modes for Rayleigh waves (central plot – Fig. 14) and one curve for the Rayleigh-wave ellipticity (right plot – Fig. 14). The two modes for Rayleigh-wave dispersion curves are interpreted as fundamental mode, the solid curve at lower velocities, and first higher mode, the dashed curve at higher velocities. Details about the technique used for the picking, the frequency range and the mode attribution can be found in Table 1.

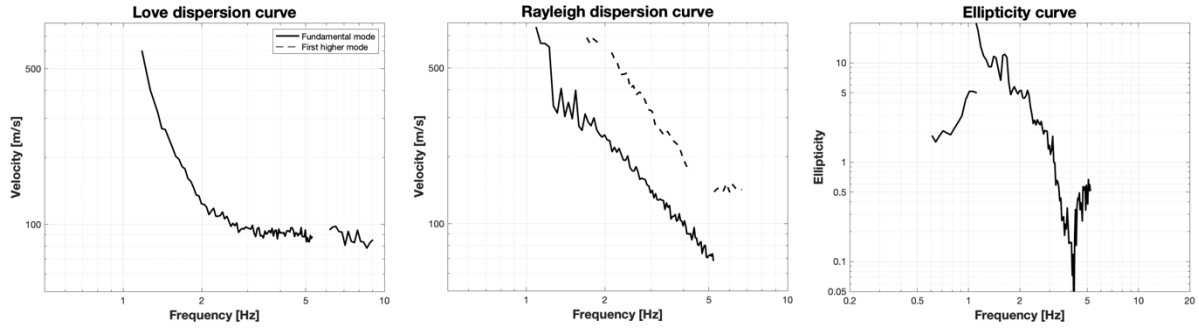

Figure 14: Overview of the dispersion curves used as target for the different inversions.

Table 1: List of the curves used as target in the inversion.

Method	Wave type	Mode	Curve type	Frequency range [Hz]
WaveDec 3C-HRFK	Love	fundamental	dispersion	1.09-5.38 6.17-9.04

WaveDec	Rayleigh	fundamental	dispersion	1.09-5.34
3C-HRFK (vert) 3C-HRFK (rad)	Rayleigh	first	dispersion	1.7-4.2 5.23-6.69
RayDec (SKES09) WaveDec	Rayleigh	fundamental	ellipticity	0.61-1.12 1.09-5.34

4.2 Inversion parameterization

For the inversion, five different parameterizations are tested. The first four involve free values of thickness and velocities for different layers, ranging from 5 to 11 layers over the half-space. The S- and P-wave velocities are allowed to range from 50 to 3500 m/s and from 100 to 7500 m/s, respectively. The deepest interfaces are allowed to range to a depth of 800 m for all four parameterizations; the density is fixed to 2500 kg/m^3 for the bedrock layer and to 2000 kg/m^3 for all the other layers.

The last parametrization (*SKESfix*) has fixed layer thicknesses and consists of 24 layers over the half-space, with the deepest interface at 800 m depth. Equal ranges are defined for the P- and S-wave velocities, while the density increases gradually for each layer from 2000 kg/m^3 to 2500 kg/m^3.

4.3 Inversion results

We performed 10 inversions for each parameterization (see Table 2) using the *dinver* routine (http://www.geopsy.org/). Each inversion run produced a total of 280000 models to assure a good convergence of the solution. Figs. 15 – 19 show the best results for each parametrization. Table 2 reports name of each performed inversion, the number of layers, the number of models, and the lowest misfit for each tested parametrization.

Table 2: List of inversions

Inversion	Number of layers	Number of models	Minimum misfit
SKES 5l	5	280000	0.406
SKES 7l	7	280000	0.408
SKES 9l	9	280000	0.423
SKES 11l	11	280000	0.433
SKES fix	24	280000	0.407

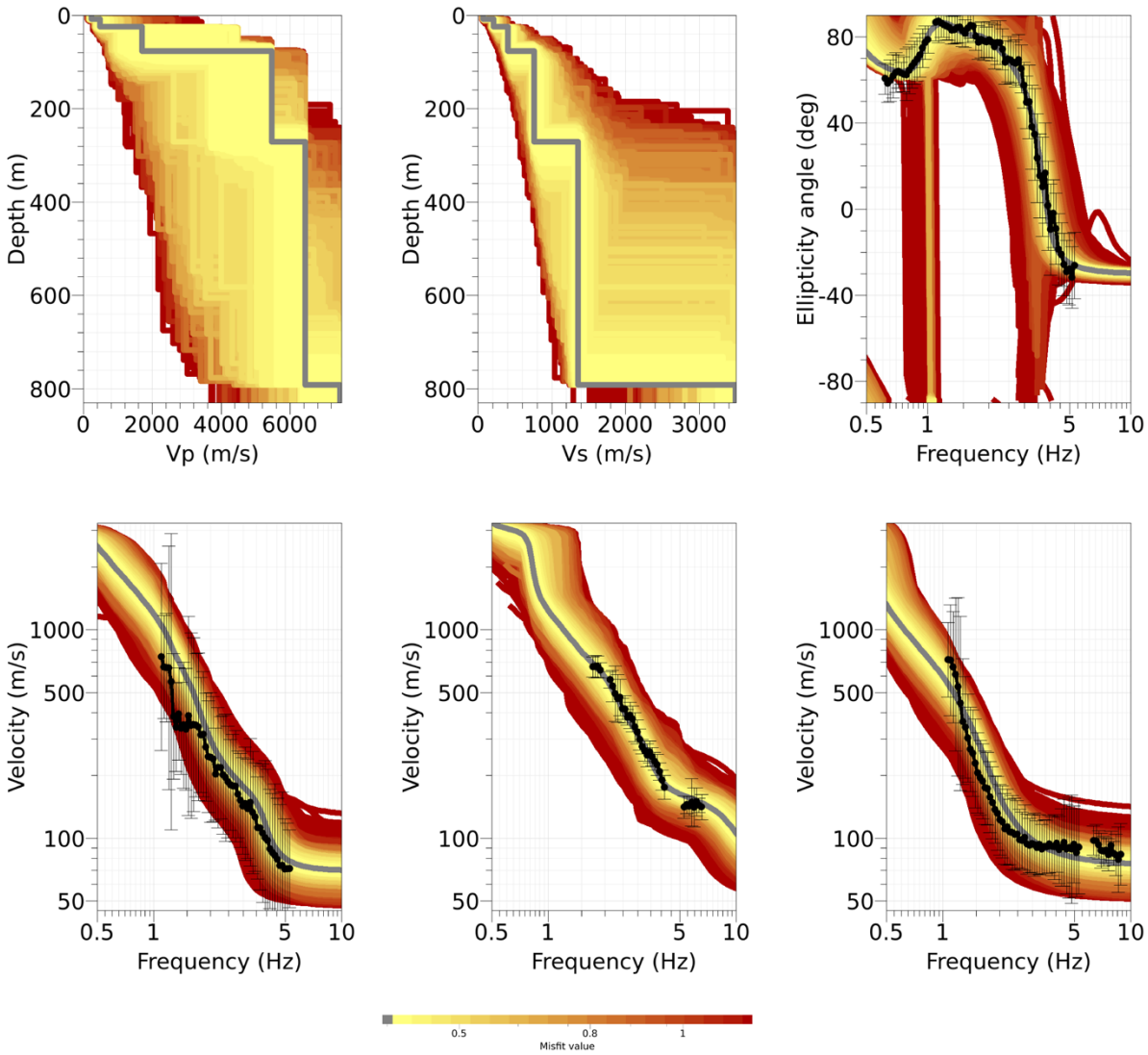

Figure 15: Inversion SKES5l. Top line: P-wave velocity profiles (left), S-wave velocity profiles (center) and Ellipticity angle curve (right). Bottom line: Dispersion curves for the fundamental and first higher modes of Rayleigh waves (left - center) and fundamental mode of Love waves (right). The black dots indicate the data points used for the inversion, the black bars the standard deviation of the inverted curve, while the gray line shows the best-fitting model.

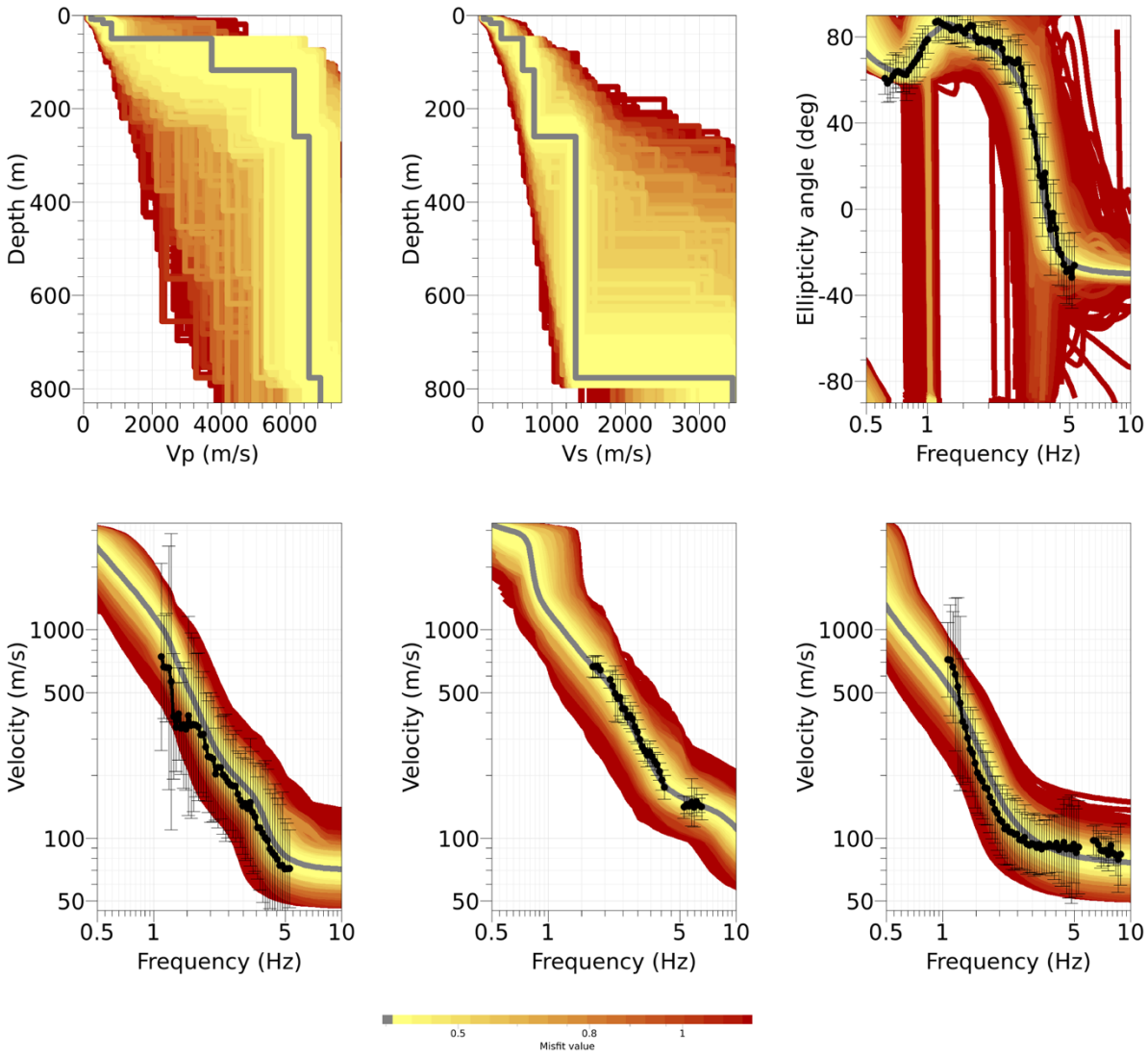

Figure 16: Inversion SKES7l. Top line: P-wave velocity profiles (left), S-wave velocity profiles (center) and Ellipticity angle curve (right). Bottom line: Dispersion curves for the fundamental and first higher modes of Rayleigh waves (left - center) and fundamental mode of Love waves (right). The black dots indicate the data points used for the inversion, the black bars the standard deviation of the inverted curve, while the gray line shows the best-fitting model.

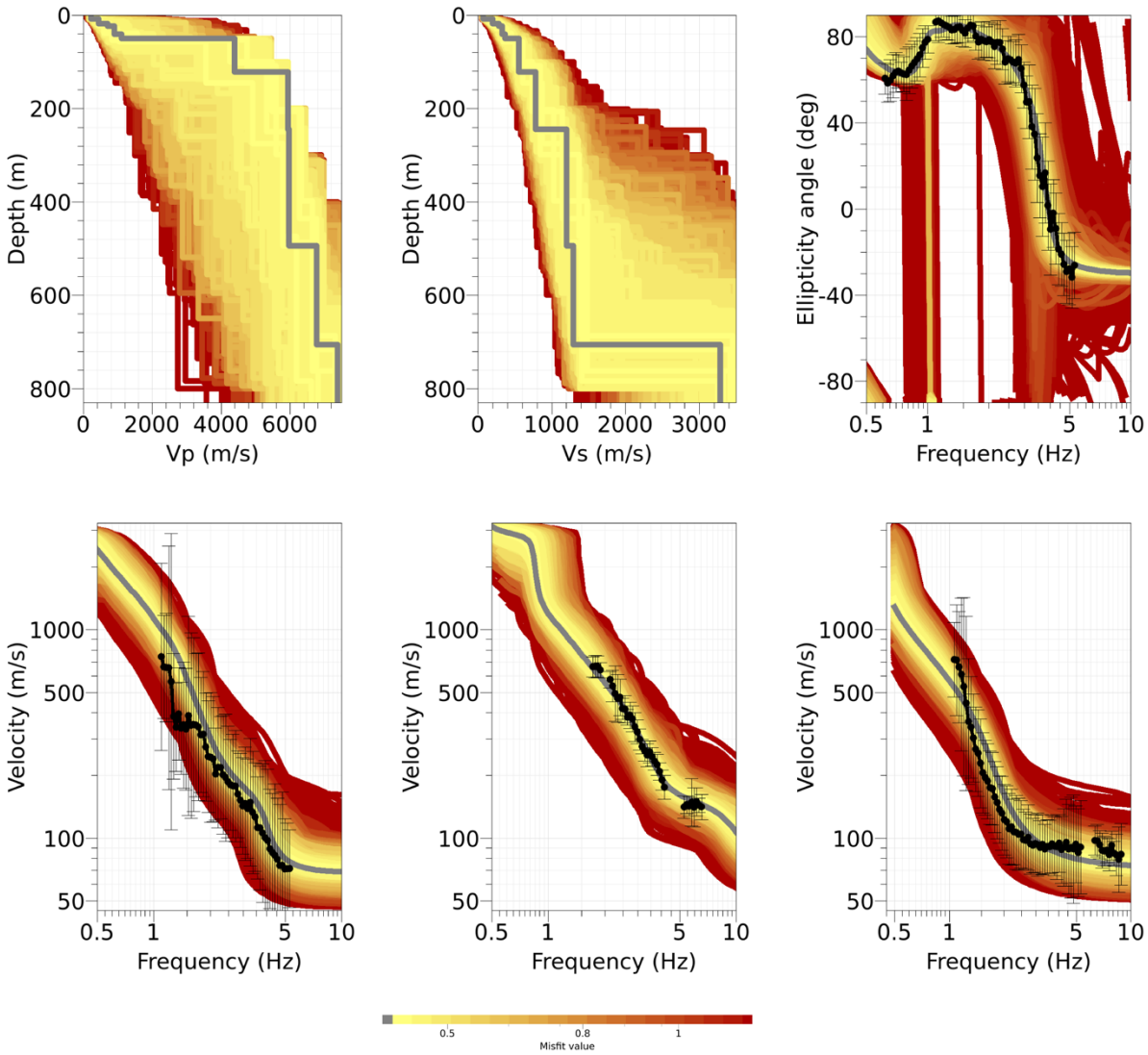

Figure 17: Inversion SKES9l. Top line: P-wave velocity profiles (left), S-wave velocity profiles (center) and Ellipticity angle curve (right). Bottom line: Dispersion curves for the fundamental and first higher modes of Rayleigh waves (left - center) and fundamental mode of Love waves (right). The black dots indicate the data points used for the inversion, the black bars the standard deviation of the inverted curve, while the gray line shows the best-fitting model.

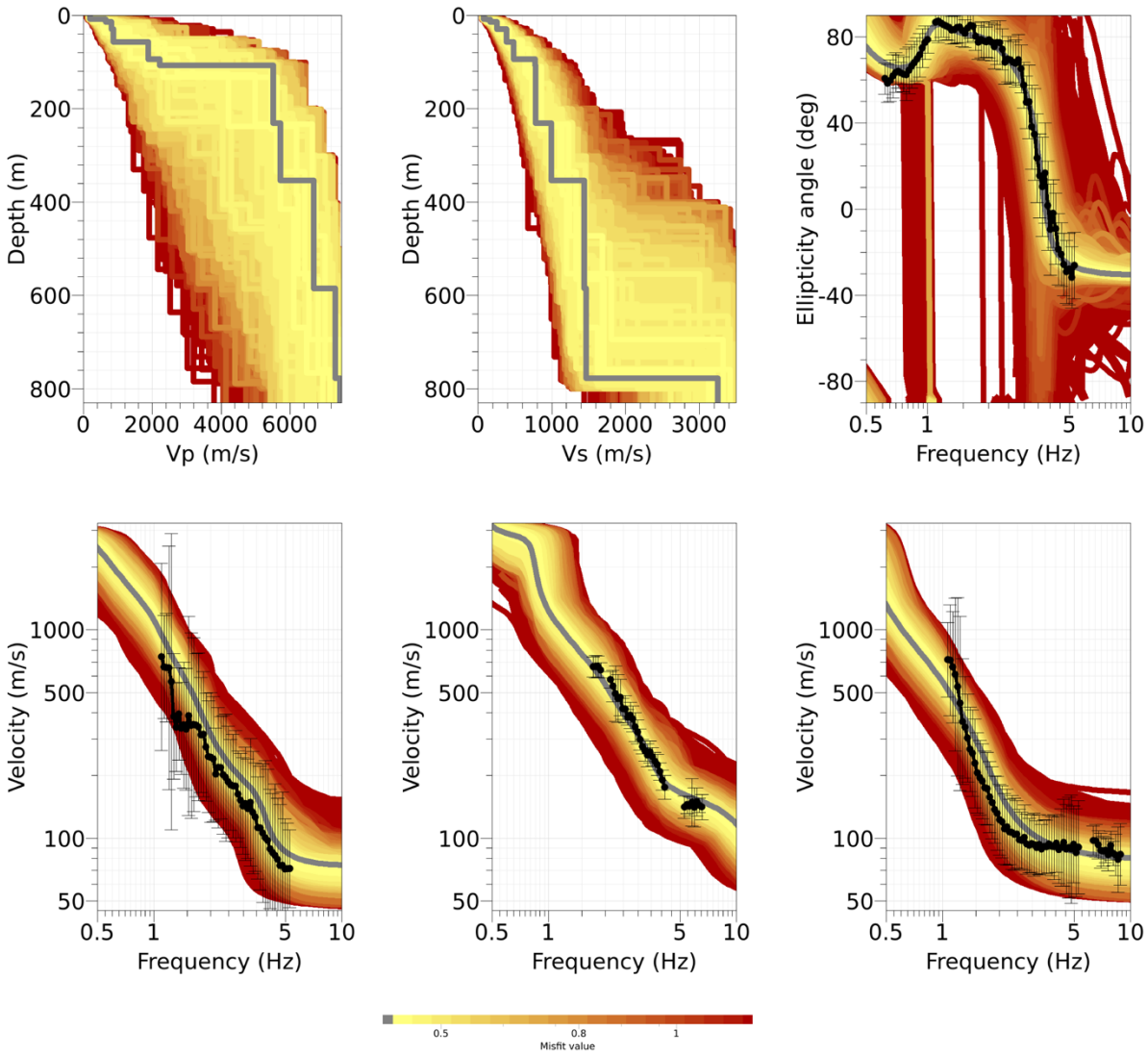

Figure 18: Inversion SKES11l. Top line: P-wave velocity profiles (left), S-wave velocity profiles (center) and Ellipticity angle curve (right). Bottom line: Dispersion curves for the fundamental and first higher modes of Rayleigh waves (left - center) and fundamental mode of Love waves (right). The black dots indicate the data points used for the inversion, the black bars the standard deviation of the inverted curve, while the gray line shows the best-fitting model.

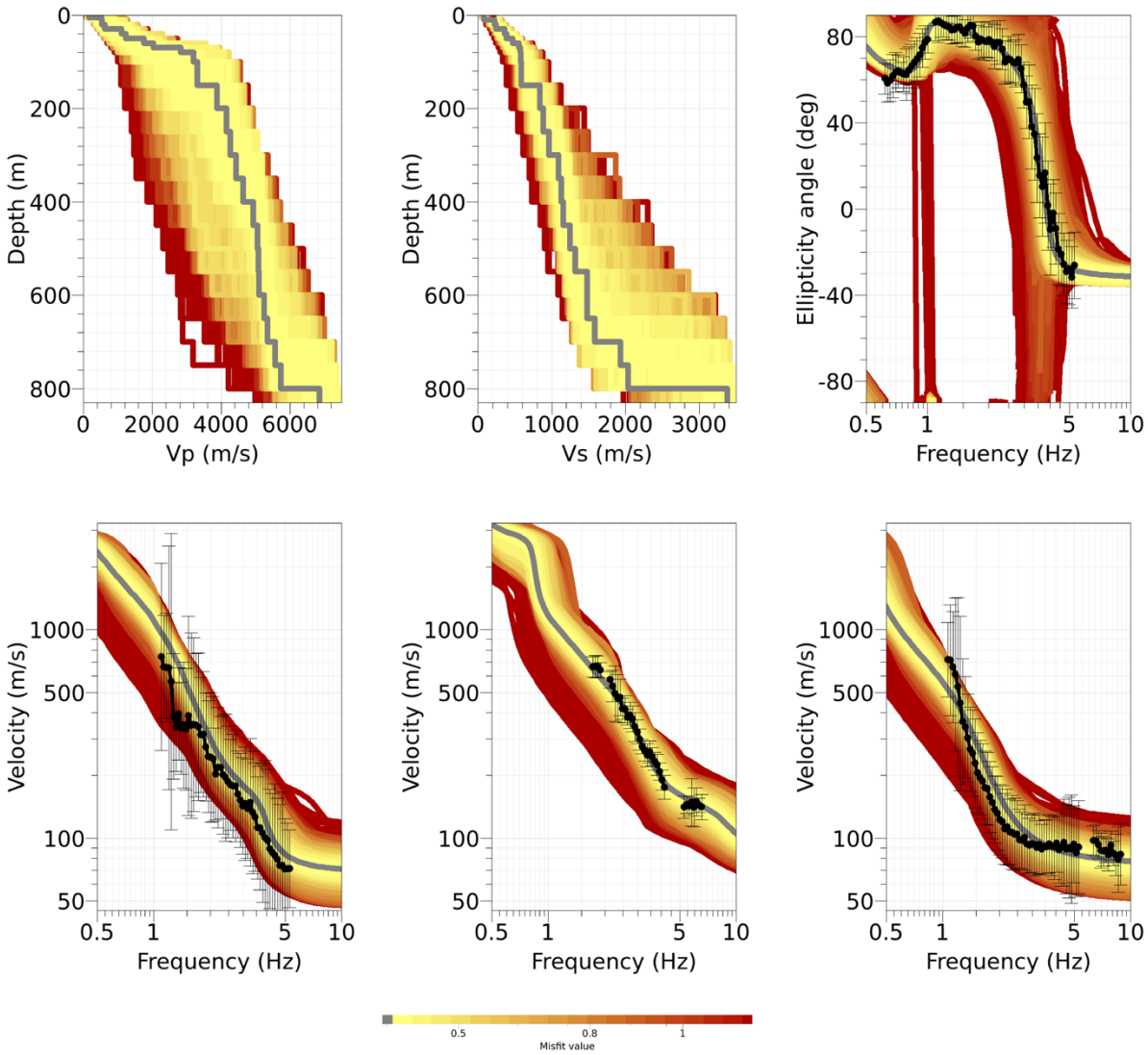

Figure 19: Inversion SKESfix. Top line: P-wave velocity profiles (left), S-wave velocity profiles (center) and Ellipticity angle curve (right). Bottom line: Dispersion curves for the fundamental and first higher modes of Rayleigh waves (left - center) and fundamental mode of Love waves (right). The black dots indicate the data points used for the inversion, the black bars the standard deviation of the inverted curve, while the gray line shows the best-fitting model.

4.4 Inversion results - Neopsy

In addition to the five inversions performed using the *dinver* routine, the inversion is also performed using the multizonal transdimentional Bayesian formulation (Neopsy – Hallo et al. 2021). The targets of the inversion are fundamental modes of Rayleigh and Love waves dispersion curves, the first higher mode of Rayleigh waves dispersion curve and the fundamental mode of Rayleigh-wave ellipticity curve. The parametrizations for the seismic velocities, density, Poisson's ratio and depth are defined within ranges: the S- and P-wave seismic velocities range from 50 to 3500 m/s and from 100 to 7500 m/s, respectively; the density adjusts between 2000 and 3000 kg/m^3, while the Poisson's ratio is set to change between 0.2 and 0.45. The maximum depth is set to 800 m and no velocity inversion is allowed. The inversion produced 5000 initial models and 25000 new models for a total of 30000 models.

The results of the inversion are shown in Figs. 20 and 21. Fig. 20 shows the fit of the measured curves used in input, while Fig. 21 displays the corresponding posterior marginal Probability Density Functions (PDF) and the resulting profiles for v_p, v_s, ρ and υ. The blue profile shows the best model using the Maximum Likelihood (ML), while magenta represents the model with the best Maximum A Posteriori (MAP) probability.

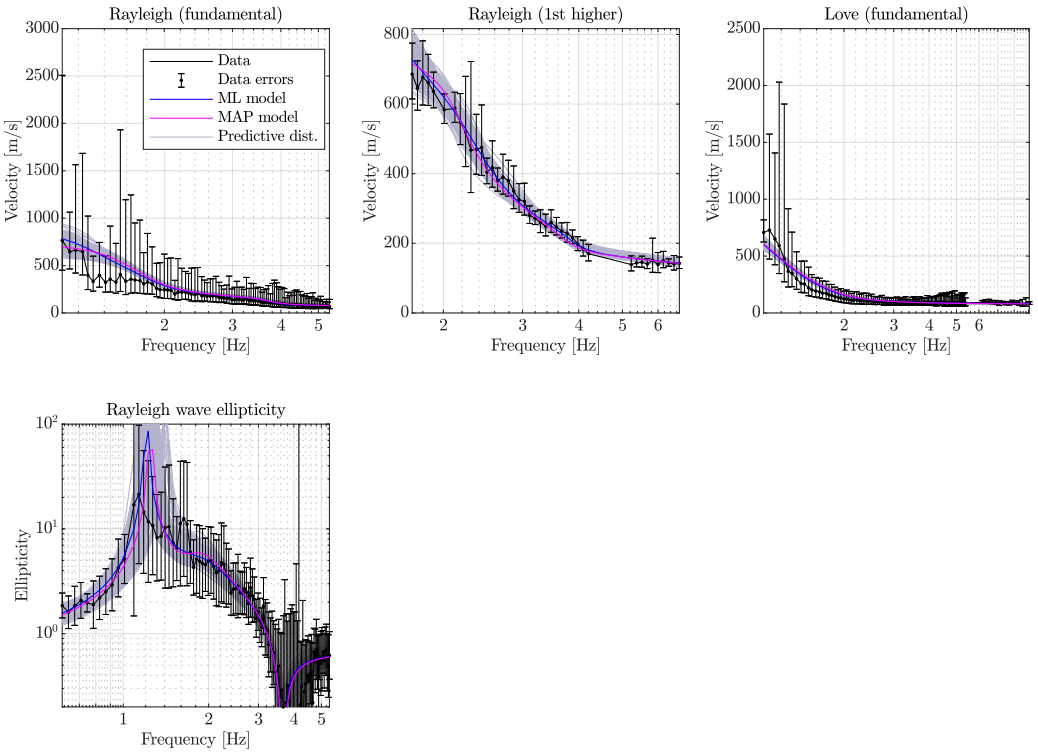

Figure 20: Results for the inversion using multizonal transdimensional Bayesian formulation. Top row: Rayleigh-wave fundamental mode (left), Rayleigh-wave first higher mode (center) and Love-wave fundamental mode (right). Bottom row: Rayleigh-wave ellipticity curve.

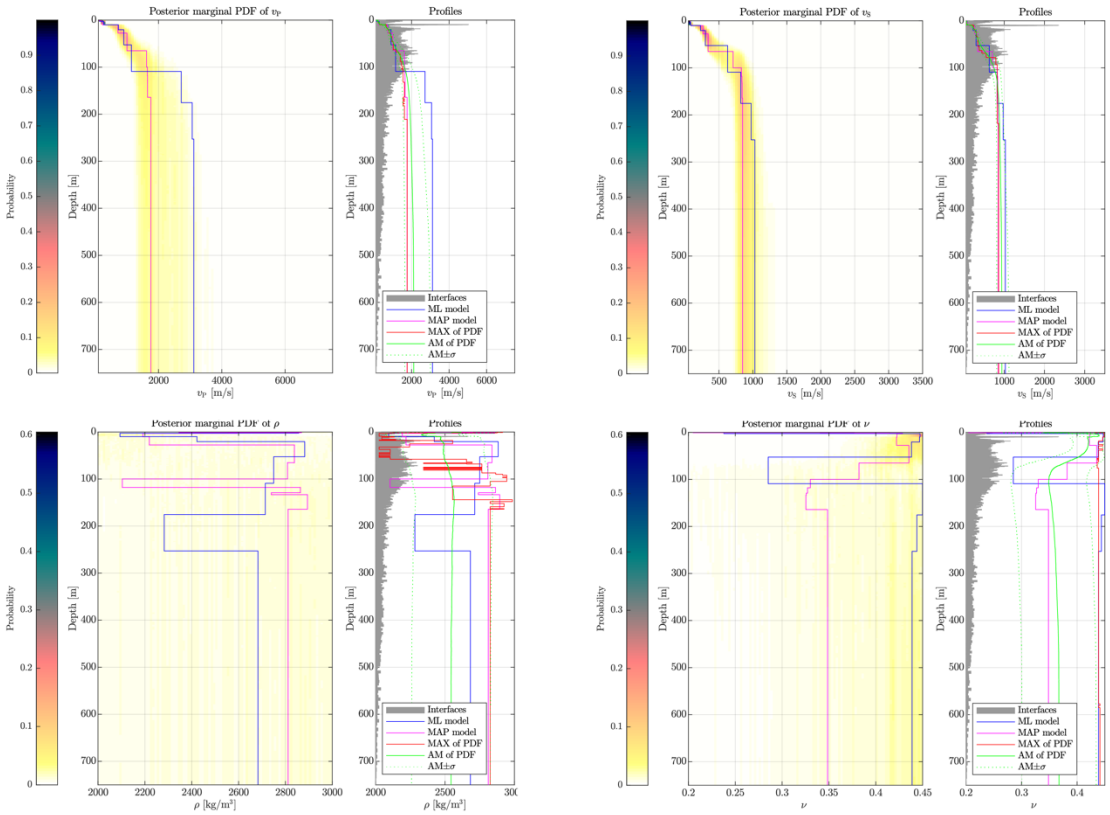

Figure 21: Posterior marginal PDF and profiles of P-waves (top left), S-waves (top right), density (bottom left) and Poisson's ratio (bottom right). Overview of the best profiles for each PDF for the Maximum Likelihood model (ML - blue) and the Maximum A Posteriori model (MAP - magenta).

4.5 Discussion of the inversion results

The velocity models with the lowest misfit are shown in Fig. 22. Results of *dinver* inversions are shown in green and grey colors, while the models from *Neopsy* are displayed in blue and magenta and correspond to the best models from the Maximum Likelihood and Maximum A Posteriori models, respectively.

Velocity profiles estimated using *dinver* show a first layer of 8 m with S-wave velocities of about 72 m/s (Fig. 22 – right plot). The bottom of this first layer is marked by a strong impedance contrast with S-wave velocities up to 215 m/s (*SKES5l*). Layers underneath present a gradual increase of S-wave velocity with depth. At 259 m, *SKES5l*, *SKES7l* and *SKES9l* models show a second velocity contrast with an increase of S-wave velocities up to 1360 m/s (*SKES5l*). *SKES11l*, which consists of 11 layers over the half-space, doesn't show such a strong velocity contrast but a gradual increase using two layers at 231 and 354 m. The last impedance contrast corresponds to the transition to the half-space. Here, all *dinver* estimated profiles have S-wave velocities between 3257 m/s (*SKES11l*) and 3500 m/s (*SKES5l*). The resolution of the subsurface and the number of strong impedance contrasts depend on the number of layers in each model. *SKES5l* model, which has only 5 layers over the half-space, shows all main contrasts; *SKES11l*, instead, is able to show a gradual increase of S-wave velocity with depth.

SKESfix, in gray color with dashed line-style, is obtained fixing the depth of each layer and allowing only the shear-wave velocity to adjust within specified ranges. As can be observed for *SKESfix*, S-wave velocity increases gradually with depth and only at the transition with the half-space, at 800 m, the S-wave velocity has a strong increase from 2035 to 3380 m/s.
MAP and ML models show a first velocity contrast at about 10 m, deeper than the *dinver* results. At 10 m, the S-wave velocity of ML model is 227 m/s equal to *SKESfix* model, while MAP model has V_s equal to 264 m/s. The S-wave velocity for both models increases gradually with depth, down to 252 for ML model (V_s = 1029 m/s) and 100 for MAP model (V_s = 848 m/s). This interface, as the last one in both velocity profiles, is interpreted as the transition with the half-space.
The velocity profiles resulting from *dinver* inversions have V_{S30} between 143.4 and 147.6 m/s, with an average value of 146.1 ± 1.77 m/s. The V_{S30} for the MAP and ML models from Neopsy inversion are 152 and 151 m/s, respectively.

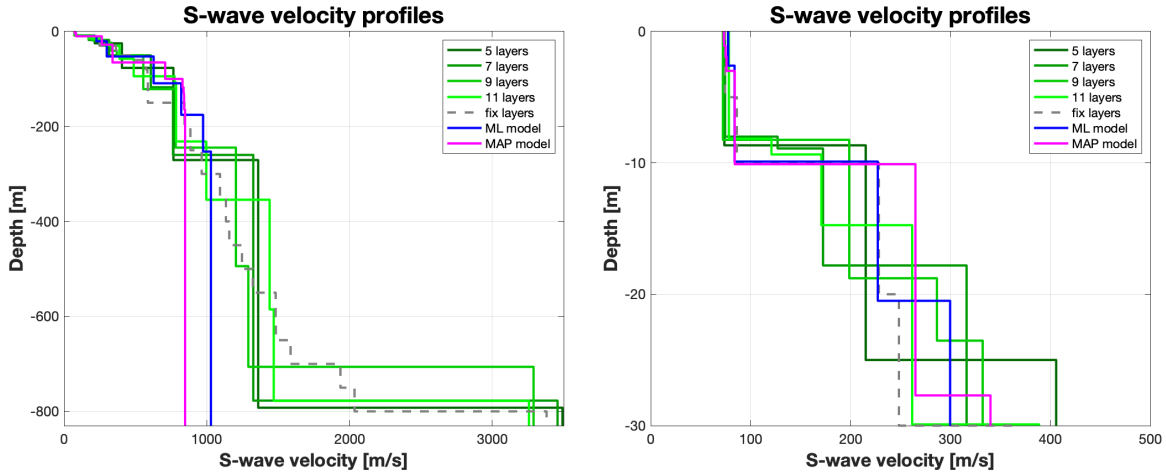

Figure 22: Overview of the best shear-wave velocity profiles of the different inversions (left) and zoom on the upper 30 m of the inversion profiles (right).

5 Further results from the inverted profiles

5.1 SH transfer function

The average theoretical shear-wave transfer functions for the best estimated models are shown in Figure 23. The SH-wave transfer functions for *dinver* (gray/black curve), MAP (magenta) and ML (blue) models are similar over the entire frequency. At low frequency, between 0.6 and 3.5 Hz, all transfer functions show a wide peak with maximum amplification of 9.6 at 1.9 Hz (*dinver* model). While the SH-wave transfer function is smooth for MAP and ML models, the curve computed using *dinver* profiles presents many narrow peaks. Above 3.5 Hz, all theoretical SH transfer functions show one peak at 6.4 Hz and one at about 10.5 Hz. Between 3.5 Hz and 30 Hz the average amplification is 3-4 with maximum of 13 at 14.1 Hz (MAP model) and minimum of 1.15 at 8.2 Hz (MAP model).
The seismic station was installed on 20 July 2023 and the passive seismic array measurement was performed on 25 July 2023. Due to the short time between the installation of the seismic station, the array acquisition and data processing, no earthquake is recorded, so no empirical amplification function is computed for SKIES station.

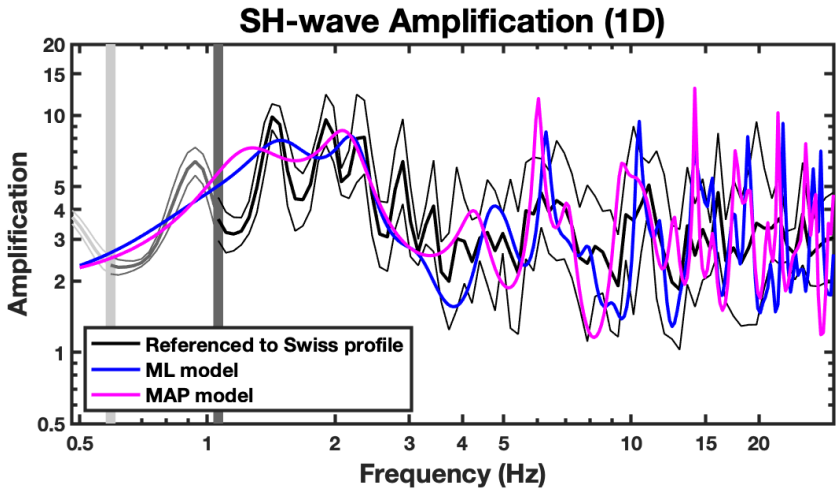

Figure 23: Modeled amplification function and standard deviation (black lines) for dinver velocity profiles. Modeled amplification functions for MAP and ML models from Neopsy inversion are shown in magenta and blue, respectively. The light grey bar shows ellipticity lower frequency value, dark grey bar indicates lower frequency value obtained with dispersion curves.

5.2 Quarter-wavelength representation

The quarter-wavelength velocity approach (Joyner et al., 1981) provides, for a given frequency, the average velocity at a depth corresponding to 1/4 of the wavelength of interest. Figure 24 shows the quarter-wavelength results using the best models of Figs. 15-19 obtained inverting the fundamental modes of Rayleigh and Love wave dispersion curves, the first higher mode of Rayleigh waves and the Rayleigh-wave ellipticity angle for the fundamental mode. The results using this proxy, considering frequency limits of the experimental data between 1 to 9 Hz for the dispersion curves and between 0.6 and 5.3 Hz for the ellipticity angle curve, is well constrained down to 136 m. The quarter-wavelength impedance contrast introduced by Poggi et al. (2012) is also displayed in the Fig. 24; it corresponds to the ratio between two quarter-wavelength average velocities, respectively from the top and the bottom part of the velocity profile, at a given frequency.

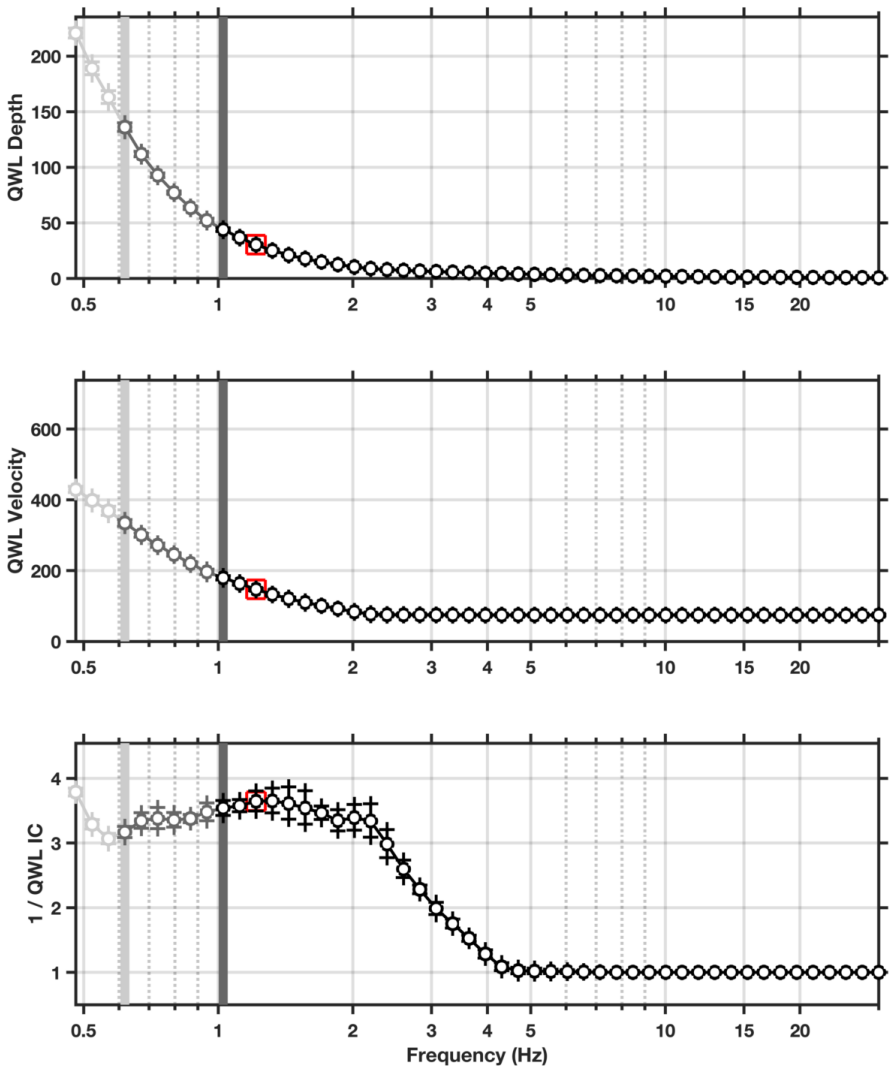

Figure 24: Quarter wavelength representation of the velocity profiles for the best models of the inversions (top: depth, center: velocity, bottom: impedance contrast). The light grey bar shows ellipticity lower frequency value, dark grey bar indicates lower frequency value obtained with dispersion curves and red square corresponds to f_{30} (frequency related to the depth of 30 m).

6 Discussion and conclusions

The passive array measurement performed in Kriens in July 2023 allowed the investigation of the subsurface underneath the SKIES permanent station.

The H/V analysis shows two peaks in the study area. The first peak, at about 1-1.1 Hz, is interpreted as the fundamental peak (f_0); the other is distributed over a wider range of frequencies (4.8-10.4 Hz) and is interpreted as the first higher mode peak (f_1). f_0 is homogeneously distributed over the study area with lower frequencies at the center of the array, in the inner rings, and slightly higher in the outer rings. f_1 is located only at the center of the array and in the north-west sector. For the

same sites, RayDec ellipticity curves are computed. These curves have shapes and amplitudes which are similar to the H/V curves.
The inversion of Rayleigh- and Love-wave dispersion curves and of the Rayleigh-wave ellipticity angle curve yields to the estimation of P- and S-wave velocity profiles investigating the subsurface down to about 800 m. *dinver* velocity profiles show two strong velocity contrasts at 8 m and at about 259 m with maximum *Vs* of 72 m/s and 1360 m/s, respectively. The transition to the half-space is located at about 800 m and it is marked by a strong increase in S-wave velocity (up to 3500 m/s). With the exception of this last interface, *Vs* increases gradually with depth.
Neopsy models have shallower resolution when compared with *dinver* results. MAP model investigates the subsurface down to 100 m (V_s = 848 m/s), while ML model down to 252 m (V_s = 1029 m/s). Both models show a gradual increase of shear-wave velocity with depth.
The V_{S30} value of the site is 147.1 m/s (*SKES11l*), corresponding to soil class D in EC8 and SIA261 classifications. V_{S30} calculated for MAP and ML models are 152 and 151 m/s, respectively.
According to the QWL interpretation, inverted dispersion and ellipticity curves accurately estimates shear-wave velocities down to 136 m. This value corresponds to a much shallower investigation depth when compared to *dinver* and *Neopsy* inversion results.
The theoretical shear-wave transfer functions for *dinver* velocity profiles predict a maximum amplification of 9.6 at 1.9 Hz. Its shape presents a rather wide peak between 0.65 and 3.5 Hz consisting of many smaller peaks followed by a constant amplification of 3. The theoretical SH-wave transfer functions computed for MAP and ML models are similar to that for *dinver* models with a smoother peak at low frequenccy. No empirical amplification function is available for comparison for SKIES permanent seismic station.

References

Burjánek, J., Gassner-Stamm, G., Poggi, V., Moore, J. R., and Fäh, D. (2010). Ambient vibration analysis of an unstable mountain slope. Geophys. J. Int., 180:820–828.

Burjánek, J., Moore, J. R., Molina, F. X. Y., and Fäh, D. (2012). Instrumental evidence of normal mode rock slope vibration. Geophys. J. Int., 188:559–569.

Fäh, D., Gardini, D., et al. (2003). Earthquake Cataloque of Switzerland (ECOS) and the related macroseismic database. Eclogae geol. Helv. 96.

Fäh, D., Wathelet, M., Kristekova, M., Havenith, H., Endrun, B., Stamm, G., Poggi, V., Burjanek, J., and Cornou, C. (2009). Using ellipticity information for site characterisation. NERIES deliverable JRA4 D4, available at http://www.neries-eu.org.

Fritsche, S., Fäh, D., Gisler, M., and Giardini, D. (2006). Reconstructing the damage field of the 1855 earthquake in Switzerland: historical investigations on a well-documented event Geophys. J. Int., 166, 719–731

Hallo, M., Imperatori W., Panzera F. and Fäh, D. (2021). Joint multizonal transdimensional Bayesian inversion of surface wave dispersion and ellipticity curves for local near-surface imaging. Geophys. J. Int., 226, Issue 1, 627-659

Hobiger, M., Bard, P.-Y., Cornou, C., and Le Bihan, N. (2009). Single station determination of Rayleigh wave ellipticity by using the random decrement technique (RayDec). Geophys. Res. Lett., 36.

Maranò, S., Reller, C., Loeliger, H.-A., and Fäh, D. (2012). Seismic waves estimation and wavefield decomposition: Application to ambient vibrations. Geophys. J. Int., 191:175–188.

Poggi, V. and Fäh, D. (2010). Estimating Rayleigh wave particle motion from three component array analysis of ambient vibrations. Geophys. J. Int., 180:251–267.

Poggi, V., Edwards, B., and Fäh, D. (2010). Characterizing the Vertical-to-Horizontal Ratio of Ground Motion at Soft-Sediment Sites. Bulletin of the Seismological Society of America, 102(6): 2741 2756.

Wathelet, M., Chatelain, L., Cornou, C., Giulio, G. D., Guillier, B., Ohrnberger, M., and Savvaidis, A., 2020. Geopsy: A User-Friendly Open-Source Tool Set for Ambient Vibration Processing, Seismological Research Letters, XX, 1–12.